Spatial Profile and Beam Composition Measurements of the University of Wisconsin Inertial Electrostatic Confinement Laboratory Ion Guns

Matthew J. Jasica[1,2,a),b)], Gerald L. Kulcinski[2], John F. Santarius[2],

1) Sandia National Laboratories
PO Box 5800, Mail Stop 1056,
Albuquerque, NM, 87185

2) Fusion Technology Institute
University of Wisconsin-Madison
1500 Engineering Dr
Madison, WI, 53706

a) Present address: Sandia National Laboratories. Research in this work by M. J. Jasica was performed at the University of Wisconsin-Madison.

b) Corresponding author: mjjasic@sandia.gov
ORCID: 0000-0001-6741-6885
Twitter: @MattJasica

Total pages: 21

Total 2-column figures: 2 (fig 5, 6)

Total 1-column figures: 8

Total tables: 0

Sandia National Laboratories is a multimission laboratory managed and operated by National Technology & Engineering Solutions of Sandia, LLC, a wholly owned subsidiary of Honeywell International Inc., for the U.S. Department of Energy's National Nuclear Security Administration under contract DE-NA0003525.

Abstract

A custom-designed and manufactured set of ion guns has been in use at the University of Wisconsin (UW) Inertial Electrostatic Confinement (IEC) laboratory for both beam fusion experiments and materials implantation experiments. For the first time, direct measurements have been made on the spatial profiles and the mass compositions of He and D ion beams produced by these guns. The results validate assumptions about the circular Gaussian spatial profiles for both He and D ion beams. Mass composition measurements of the He beam identified a pressure-dependent minimum impurity content of 15% N^+. The D beam contained relative molecular ion fractions of 58% D_3^+, 32% D_2^+, and 10% D^+ with impurities of 15% to 20% D_2O^+. A new experimental platform, the Ion Beam and Source Analyzer (IBSA) was developed to perform these experiments on the ion guns used to irradiate candidate fusion materials.

Keywords: Beam profile, ion gun, deuterium, helium, impurities

Spatial Profile and Beam Composition Measurements of the University of Wisconsin Inertial Electrostatic Confinement Laboratory Ion Guns

I. Introduction

Plasma-facing components in nuclear fusion environments will be subjected to a broad range of extreme conditions, including high heat flux, neutron damage, and particle fluxes of hydrogen and helium ions and neutrals. In magnetic confinement devices the first wall and divertor are exposed to particles ranging with energies on the orders of eV to keV and heat fluxes on the order of 20 MW m^{-2} (Ref 1). In inertial fusion energy (IFE) devices, the first wall will be exposed to particles ranging in energy from 10 keV up to 20 MeV and energies of 5.25 J cm^{-2} per target.[2,3]

Since 2009, ion implantation experiments in candidate fusion materials have been performed using a set of custom-designed and manufactured ion guns in the MITE-E (Refs. 4–7) and DAISIE (Refs. 8–10) facilities at the University of Wisconsin-Madison (UW) Inertial Electrostatic Confinement laboratory (IEC). These guns, designed and manufactured by Egle[11], were based on an experiment by Hirsch[12]. These guns have successfully demonstrated operation with both deuterium (D) and helium (He, assumed pure ^{4}He) beams and have achieved accelerating voltages up to 150 kV, beam currents of up to 3.5 mA (Ref. 11) and ion current resolutions of ±10 μA (Refs. 4,10). The ion source is driven by filament-assisted electrons. A series of electrostatic lenses extract, focus, and accelerate the beam to the target. No magnetic filtering or steering is inherent in this gun design and is typically not implemented in the implantation systems due to hardware limitations[4,10]. More detailed treatments of the ion gun source physics and optics are given by Egle[11] and Garrison et al.[4]

An accurate knowledge of beam parameters, including spatial charge distribution and mass-to-charge ratio of the ions in the beam, is necessary to calculate derived quantities, such as the ion fluence received by an implanted sample. Historically, either indirect measurements and/or assumptions have often been made about these parameters. Specifically, the beam spatial distribution profiles of the ion guns have been previously assumed to have a stepped profile[5] or a smooth Gaussian profile[6], and the beam was assumed to contain only a single species based on the feed gas used in lieu of measurements of the mass profile. While He can form both singly and doubly ionized species, their respective ionization rates[13] combined with the low ionization fraction of the filament ion sources, on the order of 10^{-4} (Ref. 11), have often encouraged the assumption that a helium beam was composed solely of He^+. In the case of deuterium (D) or other hydrogen isotopes, this matter is complicated further by the creation of multiple molecular ion species, i.e. D^+, D_2^+, and D_3^+. Boris and Emmert[14] developed a rate equation model that was found to be in good agreement with the experimentally-measured fractions of these species in the UW IEC devices. However, both the hardware differences between ion guns and IEC devices preclude the use of such tools in assessing the molecular species present in an ion gun. In the case of ion implantation experiments, variations in these values can have a significant impact on the conversion of the measured beam current to the actual ion flux and beam species energy distribution received at a given location.

II. Methods

II.A. The Ion Beam and Source Analyzer Platform Overview

A standalone test platform at the UW-IEC laboratory, the Ion Beam and Source Analyzer (IBSA) was designed for performing analysis of the ion beam characteristics of the ion guns[11]. One significant challenge in the development of this platform was the high voltage treatment of either

the source or diagnostic regions. All prior experiments had operated the source regions of the guns at ground potential with the lenses and materials stage and diagnostics at high negative potentials (on the order of 30 kV). However, due to the operational and hardware demands of the beam diagnostic equipment, it was determined that it would be easier to operate the IBSA platform with the ion source at a high positive potential, with the diagnostics at the ground potential. Consequentially, all systems related to the operation of the ion gun and sources had to be isolated for high voltage use. These included all electrostatic lens supplies, filament supplies, gas delivery, and source cooling systems. The platform itself was demonstrated to standoff potentials of at least 50 kV without operating the ion gun. A Glassman High Voltage PS/WG-20P-15-M3 power supply was used to elevate the platform to a maximum of +20 kV for this work. Gases used in this work included 99.9995% purity He and 99.96% purity D_2.

II.B. Ion Guns Parameters

The ion gun used in the IBSA and its major components are shown in Figure 1. Two Gamma High Voltage Research DC supplies, Model RR-15-5N/M1030, were used to set the extraction and focus lens voltages. An HP 6035A power supply (0 VDC to 500 VDC, 0 A to 5 A) was used to control the filament heating voltage. An HP 6038A power supply (0 VDC to 60 VDC, 0 A to 10 A) was used to control the filament bias voltage. All power supplies were isolated on the high voltage platform and wired such that their "ground" was connected to the positive platform potential. Typical operating voltages (relative to the platform potential) for the IBSA runs were -6 kV on the extraction lens and -1.8 kV on the focus lens, relative to the positive platform potential. Typical operating filament voltages were 90 V filament heating voltage and 60 V filament bias. An insulating extension arm was used to operate the filament heating supply while the platform and supply were energized, allowing live control over the ion gun current. It was found that for these

operating conditions a maximum filament voltage of 90 V to 95 V could be obtained before reaching the Child-Langmuir limit, at which the extracted current through the ion source's plasma boundary is reduced by the space charge repulsion of the extracted particles.

II.C. Diagnostics

The primary diagnostic for measuring the beam current is a Faraday cup, shown in Figure 1b (as installed on the IBSA) and Figure 3 based on design principles discussed by Zhang[15]. The cup features a 19 mm diameter aperture and a grounded shield to protect the collecting surface of the cup from secondary electrons generated by the beam striking the walls of the beam line. Suppression of secondary electrons was accomplished with the suppression lens held at a voltage of -40 V. As with the other diagnostics discussed here, the Faraday cup was operated at ground potential. Stable current readings with a sensitivity of ±2 nA were obtained with this design.

Multiple methods can be employed to develop a beam current density profile. While 2-D methods that raster across the entire beam spot are most accurate, considerably faster and simpler 1-D methods can be used with reasonable accuracy, including a straight-edge probe, thin wire probe, double probe, or mask with a thin slit backed by a detector such as a Faraday cup[16–20]. For this work, a slit of 1 mm width and 25 mm length was machined into an aluminum mask and mounted on a linear motion vacuum feedthrough with a range of motion of 50 mm. The slit length was selected to be wider than the estimated beam spot diameter of 8 mm estimated from previous work[4,5]. The spatial scanning diagnostic is shown in Figure 4. Scans of the beam in both x and y directions can be used to determine the approximate 2-D beam spatial profile.

A magnetic separation stage, shown in Figures 1b and 2, was used to separate the ion beam into its constituent species based on their mass-to-charge (m/q) ratio. Two 6032A Agilent power

supplies in parallel delivered up to 20 A of current to a GM 5403 electromagnet to create magnetic fields of up to 45 G. The Faraday cup was mounted on a bending arm and at the end of the beamline. By sweeping the magnetic field while the beam is operating, a spectrum of peaks, each representing a unique m/q, as a function of the magnetic field B. It was assumed that the magnetic field was unidirectional and that the beam was orthogonal to the magnetic field, which is reasonable for the geometry of the IBSA and electromagnet. Based on these assumptions, a relationship between the centroid of the peaks and m/q can be derived:

$$\frac{m}{q} = \frac{(Br)^2}{2V} \tag{1}$$

where r is the ion radius of curvature caused by the bending arm and V is the accelerating lens voltage relative to ground. For acceleration lens voltages of 20 kV this analyzer is capable of separating species with m/q of up to 55, allowing for the detection of species as heavy as argon or carbon dioxide. An XTorr 1000 residual gas analyzer (RGA) is used to supply supplemental information on gas constituents both for the background gas and the fill gas while the beam is running.

III. Results

III.A. Spatial Profiling

Spatial profiles in the x and y directions for the He beam and D beam are shown in Figure 5. Both profiles were taken using an accelerating lens voltage of 20 kV, a filament bias of 60 V, and a filament heating voltage of 85 V. Chamber pressures were 1×10^{-4} Torr and 2×10^{-4} Torr for the

He and D beams, respectively. A Gaussian distribution is fitted to the measured profiles and fits each of these profiles reasonably well, validating prior assumptions of a Gaussian ion distribution.

III.B. Ion Composition Profiling

Mass-to-charge (abbreviated as "mass") profiles for He over a range of accelerating voltages and pressures are shown in Figure 6a and Figure 6b, respectively. The radius of curvature r was unable to be precisely determined, so equation 1 for estimating mass peaks from the magnetic field was calibrated for $m/q = 4.0$ at $B = 1215$ G and V = 20 kV. As only two mass peaks are expected for pure ^{4}He ($m/q = 4.0$ for He^+ and $m/q = 2.0$ for He^{2+}), interpretation of this spectrum is rather straightforward to interpret and suitable for a calibration point. The MATLAB® Curve-Fitting Toolbox[26] was used to analyze multiple peaks in a spectrum and determine the centroid of each peak B. As shown in Figure 6a, the peaks at the lower voltages are in good agreement with their predicted value from equation 1. While the magnet is capable of higher field strengths, no significant signals were measured above the domain plotted. An additional peak around $m/q = 14$ was also observed, believed to be nitrogen (N), as discussed later. A small peak at $m/q = 1$ is present in all scans due to the presence of background hydrogen in the vacuum system.

Mass scans for the D beam at multiple accelerating voltages and a pressure of 1×10^{-4} Torr are shown in Figure 6c. Scans at multiple pressures and an accelerating voltage of 20 kV are shown in Figure 6d. Peaks for the multiple molecular D ion species at mass 2, 4, and 6 align nicely with the predicted fields from equation 1, and smaller peaks at masses 1 (H^+) and 3 (HD^+) are also observed. A wide peak is observed around mass 20 to 25 and is believed to be D_2O, as discussed later. A closer examination of the low m/q peaks is shown in Figure 7.

IV. Discussion

IV.A. Spatial Profiling

A Gaussian approximation fits each of the spatial profiles in Figure 5 reasonably well. An asymmetry in the y-axis scan is observed for both the D and He beams. This is likely due to an unintended tilt in the gun axis relative to the Faraday cup and slit axes created during the manual assembly of the gun chamber. This may also account for the different measured beam widths between the x and y axis for each species. Optical measurements of the beam spot on samples[4,5,8] have confirmed a radially symmetric beam spot, so the measured asymmetry in this work is likely due to the IBSA setup as opposed to an inherent quality of the ion gun.

It is important to point out that these measurements do not have the same physical meaning as the beam current density. Rather, the measured current $I(x)$ is the integrated signal over the entire width y of the beam that passes through the slit. Integral transforms and numerical methods can be used to reconstruct the current density profile from these measurements. However, the transforms of a circular Gaussian profile also yield a Gaussian current density profile[16].

Care should be taken when comparing the measured width of the beam in the IBSA to the beam spot sizes produced by similar guns reported in MITE-E (Refs. 4–7) or DAISIE (Refs. 8–10). The distance from the accelerating lens to the Faraday cup in the IBSA is 500 mm, while the distance from the cathode lens to the target in DAISIE is only 60 mm, so the divergence of the beam must be considered. While the divergence was not measured for this work, future tests could site the slit analyzer at multiple distances along the beam line to measure the divergence, allowing for quantitative predictions of the beam spot size in future experiments.

IV.B. Ion Composition Profiling

Integrating the total counts under each of the peaks yields the relative composition of each ion species. A decrease in the He composition with increased pressure at constant voltage is observed in Figure 8. The He fraction in the beam is approximately 86% at 3.1×10^{-5} Torr and decreases to as low as 12% at 2.2×10^{-4} Torr. Figure 9 demonstrates an increase in He fraction with increased voltage, however this effect is less significant at lower pressures where the He fraction is already high. A higher voltage corresponded to an increased total current collected. Together, these suggest that energy-dependent reactions with neutral background species along the beam line, where the electric field structure is highly dependent on the accelerating lens potential, drive the impurity formation process. However, some caution must be taken with this interpretation, as the mean free paths for beam-background interactions (discussed below) at these pressures are on the order of 10^5 cm, which is significantly larger than the device dimensions.

The impurity peak around mass 14 is believed to be N^+ or N_2^{++}. Other nearby mass candidates could include O (mass 16) or H_2O (mass 18); however, residual gas analyzer (RGA) measurements indicate nitrogen as the most significant species present in the background constituents for the He fill gas. At this time, the mechanism for producing these impurity ions in the beam in significant quantities and the observed trends is not well understood. Possible sources for the nitrogen may be vacuum background constituents or adsorbed nitrogen on the tungsten filament in the ion source. Nitrogen is also present in the boron nitride insulating spacers in the ion gun, however the geometry of the gun is unfavorable for collisions between the ions with the spacers. Atomic and molecular processes including Penning ionization or charge exchange, which have significant cross-sections at the energies around 5 kV to 20 kV (Refs. 21–25), may be responsible for the creation of nitrogen ions from reactions with the helium ions.

Turning to deuterium beams and integrating the mass 2, mass 4, and mass 6 peaks yields average relative D_i^+ fractions of 10% D^+, 32% D_2^+, and 58% D_3^+ at implantation-relevant pressures of 1×10^{-4} Torr to 2×10^{-4} Torr. At these pressures the fraction of impurities ranges from 15% to 20%. As was the case with He, an increase in pressure corresponded with an increase in impurity content although not to the same extent, as shown in Figure 10. This also corresponded with an increase in the amount of D_3^+ and reduction in D_2^+ as the pressure increased. This is due to the dominance of the D_2^+-D_3^+ interchange reaction dominating these conditions in the weakly ionized D plasma[14]. Unlike the He plasma, the impurity fraction is relatively independent of the accelerating lens potential. This suggests the reactions driving the impurity formation process are occurring in the source region, where the electric field structure is also insensitive to the accelerating lens potential.

RGA measurements suggest this impurity peak of *m/q* of 20 to 25 is most likely mass 20 and is believed to be D_2O^+. Light water is the largest background constituent in the IBSA. Dissociation and formation atomic and molecular reactions can lead to the formation of D_2O from D_2 and H_2O. While this does not align as closely with the mass peak predicted by equation 1, it is the most plausible candidate for this range considering the fill gas and observed background constituents of H_2O, N_2, O_2, He, and CO_2. The formation of impurity ions is relatively insensitive to accelerating voltage but exhibited a tendency to increase with increasing pressure. In the context of materials implantation experiments, the relative D species mix given above indicates that for every D ion measured, an average of 2.5 D atoms were implanted in the sample.

It is assumed that each of the low *m/q* peaks in Figure 6 corresponds to a single ion species. At those *m/q* the only predicted overlaps are at *m/q* = 2 (D^+ and He^{++}) and *m/q* = 4 (D_2^+ and He^+). Chamber purges using the new fill gas and RGA sweeps were performed in between experiments

using He and D to verify that minimal residual gas from prior experiments remained. From Figure 6a and Figure 6b the measured He^{++} fraction in the He spectrum is negligible, and it is assumed that even less He^{++} would be expected in the D spectrum. It is also assumed that no D species are present in the He spectrum, as Figure 6c and Figure 6d imply that any D_2^+ would be accompanied by a larger fraction of D_3^+. One more assumption is that the ions enter the mass analyzer at the full acceleration potential. Depending on where these interactions are occurring along the beam, ions may enter the mass analyzer at a lower energy, implying the measurement of heavier masses than those discussed here.

V. Conclusions

Spatial and mass analysis was performed for the first time on the ion gun beams used by the UW-IEC laboratory. Spatial profile measurements validate the assumption of a circular Gaussian profile as a good approximation. Mass analysis indicates that all the He ions in the He beam are singly-ionized He. The D beam was found to contain a significant amount of both D_2^+ and D_3^+, resulting in an average of 2.5 D atoms per molecular ion in the beam. Impurity fractions in both beams were found to depend on pressure. The impurities He beam were also sensitive to the accelerating potential energy, while impurities in the D beam were relatively insensitive to it. At conditions relevant to implantations that use these guns, that is lower pressure and higher voltage, the impurity concentrations are at their minimum levels of approximately 15% to 20% for both the He and D beams. The modular design of the IBSA platform allows for future testing of additional gases, beam diagnostics, or ion guns beyond what was discussed in this work.

The presence of impurities and multiple molecular ion species in these ion beams raises additional interesting areas of exploration, particularly into the physics of why certain species are formed and where these interactions are occurring in the system. These impurities may also adjust the

behaviors, such as surface morphology formation or mass loss, observed in previous materials implantation experiments performed using these ion guns, but the effects of these beams as compared to pure beams is currently unknown. Since they cannot be easily removed via magnetic filtering in the current applications of the beams, further study is needed to determine optimal source, lens and pressure conditions for minimizing their presence. Additional techniques, such as ion beam analysis, x-ray photoelectron spectroscopy, or glow-discharge optical emission spectroscopy would provide valuable information on the specific atoms and impurities being implanted by these ion guns. Given the trends observed in this work, these values are believed to represent an upper limit on the impurity content in previous and ongoing implantation experiments at the UW-IEC Fusion Laboratory.

Acknowledgements

This work has been funded in part by the University of Wisconsin-Madison, the Grainger Foundation, the Greatbatch Foundation, and TAE Technologies. Special thanks go to Richard Bonomo and Aaron Fancher for their collaboration in developing the high-voltage aspects of the IBSA.

Sandia National Laboratories is a multimission laboratory managed and operated by National Technology and Engineering Solutions of Sandia, LLC, a wholly owned subsidiary of Honeywell International, Inc., for the U.S. Department of Energy's National Nuclear Security Administration under contract DE-NA0003525.

This paper describes objective technical results and analysis. Any subjective views or opinions that might be expressed in the paper do not necessarily represent the views of the U.S. Department of Energy or the United States Government.

References

1. Y. UEDA et al., "Simultaneous irradiation effects of hydrogen and helium ions on tungsten," J. Nucl. Mater. **386–388**, 725 (2009); https://doi.org/10.1016/j.jnucmat.2008.12.300.

2. J. D. SETHIAN et al., "The science and technologies for fusion energy with lasers and direct-drive targets," IEEE Trans. Plasma Sci. **38** 4 PART 2, 690 (2010); https://doi.org/10.1109/TPS.2009.2037629.

3. J. D. SETHIAN et al., "An overview of the development of the first wall and other principal components of a laser fusion power plant," J. Nucl. Mater. **347** 3, 161 (2005); https://doi.org/10.1016/j.jnucmat.2005.08.019.

4. L. M. GARRISON et al., "The materials irradiation experiment for testing plasma facing materials at fusion relevant conditions.," Rev. Sci. Instrum. **87** 8, 083502 (2016); https://doi.org/10.1063/1.4959201.

5. S. J. ZENOBIA, L. M. GARRISON, and G. L. KULCINSKI, "The response of polycrystalline tungsten to 30keV helium ion implantation at normal incidence and high temperatures," J. Nucl. Mater. **425** 1, 83 (2012); https://doi.org/10.1016/j.jnucmat.2011.10.029.

6. L. M. GARRISON and G. L. KULCINSKI, "Irradiation resistance of grains near {0 0 1} on polycrystalline tungsten under 30 keV He+ bombardment at 1173 K," Phys. Scr. **T159** T159, 014020, IOP Publishing (2014); https://doi.org/10.1088/0031-8949/2014/T159/014020.

7. L. M. GARRISON, F. W. MEYER, and M. E. BANNISTER, "The influence of microstructure on deuterium retention in polycrystalline tungsten," Fusion Sci. Technol. **72** 4, 574, Taylor & Francis (2017); https://doi.org/10.1080/15361055.2017.1352431.

8. M. J. JASICA, G. L. KULCINSKI, and J. F. SANTARIUS, "Preliminary results of he implantation in tungsten at angled incidence in DAISIE," Fusion Sci. Technol. **72** 4, 719, Taylor & Francis (2017); https://doi.org/10.1080/15361055.2017.1350482.

9. M. J. JASICA, G. L. KULCINSKI, and J. F. SANTARIUS, "Periodic Surface Morphology Characteristics of Tungsten Under Simultaneous Helium and Deuterium Bombardment at 30 keV," Fusion Sci. Technol. (2019); https://doi.org/10.1080/15361055.2019.1602397.

10. M. J. JASICA, G. L. KULCINSKI, and J. F. SANTARIUS, "The Dual Advanced Ion Simultaneous Implantation Experiment for Testing Plasma-Facing Components of Nuclear Fusion Devices," Rev. Sci. Instruments, Submitt. (2019).

11. B. J. EGLE, "Nuclear fusion of advanced fuels using converging focused ion beams," University of Wisconsin-Madison (2010).

12. R. L. HIRSCH, "Inertial-Electrostatic Confinement of Ionized Fusion Gases," J. Appl. Phys. **38** 11, 4522, AIP Publishing (1967).

13. R. K. JANEV et al., *Elementary processes in hydrogen-helium plasmas: Cross sections*

and reaction rate coefficients, in Research supported by DOE **4**, Springer Berlin Heidelberg, Berlin, Heidelberg (1987); https://doi.org/10.1007/978-3-642-71935-6.

14. D. R. BORIS and G. A. EMMERT, "Composition of the source region plasma in inertial electrostatic confinement devices," Phys. Plasmas **15** 8, 83502, American Institute of Physics (2008); https://doi.org/10.1063/1.2965148.

15. H. ZHANG, *Ion sources*, Science Press (1999).

16. S. UGNIEWSKI, "Analysis of Straightedge, Wire, and Double Wire Probe Data for Determining Electron or Ion-Beam Profile," J. Electrochem. Soc. **125** 3, C152 (1978).

17. P. N. OSTROUMOV et al., "Design and test of a beam profile monitoring device for low intensity radioactive beams," Rev. Sci. Instrum. **73** 1, 56 (2002); https://doi.org/10.1063/1.1419227.

18. H. J. YOU, S. O. JANG, and W. I. CHOO, "Beam Profile Measurements With a Slit - Faraday Cup and a Wire Scanner for a Newly Developed 18 Ghz Superconducting Ecr Ion Source and Its Lebt," in 4th International Beam Instrumentation Conference (IBIC2015), Melbourne, Australia, 13-17 September 2015, pp. 113–117, JACOW, Geneva, Switzerland (2015).

19. J. LOPES et al., "Ion Beam Monitoring Over a Biased Target," IEEE Trans. Plasma Sci. **45** 10, 2767 (2017); https://doi.org/10.1109/TPS.2017.2735918.

20. R. B. FAIR, "A wide slit scanning method for measuring electron and ion beam profiles," J. Phys. E. **4** 1, 35, IOP Publishing (1971); https://doi.org/10.1088/0022-3735/4/1/008.

21. R. C. BOLDEN et al., "The measurement of Penning ionization cross sections for helium 23S metastables using a steady-state flowing afterglow method," J. Phys. B At. Mol. Phys. **3** 1, 61, IOP Publishing (1970); https://doi.org/10.1088/0022-3700/3/1/014.

22. T. UENO and Y. HATANO, "Measurement of the rate constant of the penning ionization of nitrogen by helium metastable states as studied by pulse radiolysis," Chem. Phys. Lett. **40** 2, 283, North-Holland (1976); https://doi.org/10.1016/0009-2614(76)85079-8.

23. C. F. BARNETT and P. M. STIER, "Charge exchange cross sections for helium ions in gases," Phys. Rev. **109** 2, 385, American Physical Society (1958); https://doi.org/10.1103/PhysRev.109.385.

24. H. C. HAYDEN and N. G. UTTERBACK, "Ionization of Helium, Neon, and Nitrogen by Helium Atoms," Phys. Rev. **135** 6A, A1575 (1964); https://doi.org/10.1103/PhysRev.135.A1575.

25. H. MARTÍNEZ and B. E. FUENTES, "Absolute differential and total cross sections for N + formation from the interaction of N 2 + with He and Ar," in Nuclear Instruments and Methods in Physics Research, Section B: Beam Interactions with Materials and Atoms **241** 1–4, pp. 459–464, North-Holland (2005); https://doi.org/10.1016/j.nimb.2005.07.056.

26. "MATLAB and Curve Fitting Toolbox Release 2017b," Natick, Massachusetts, United States.

Figures

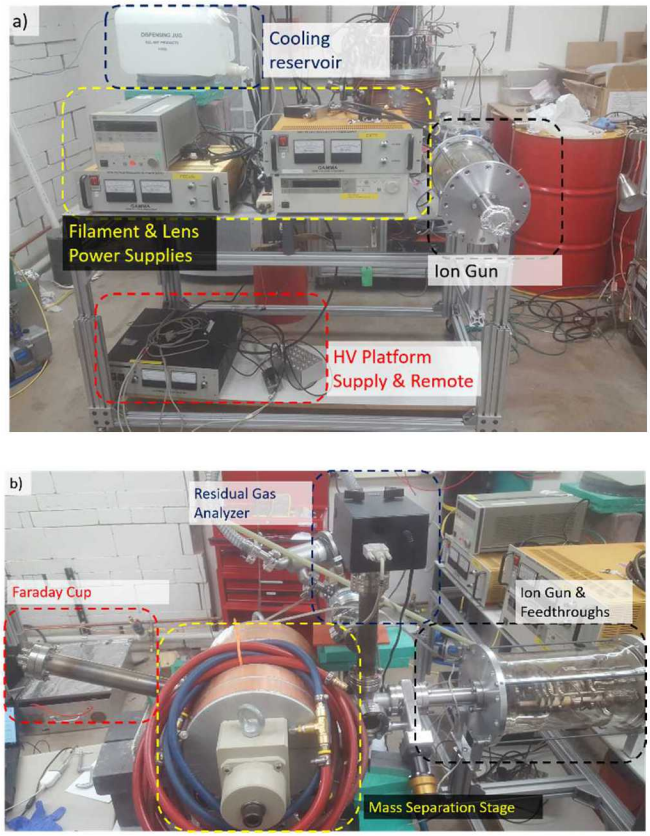

Figure 1: (top) IBSA cart and major systems. (bottom) Mass analyzer and Faraday cup diagnostics attached to beam output.

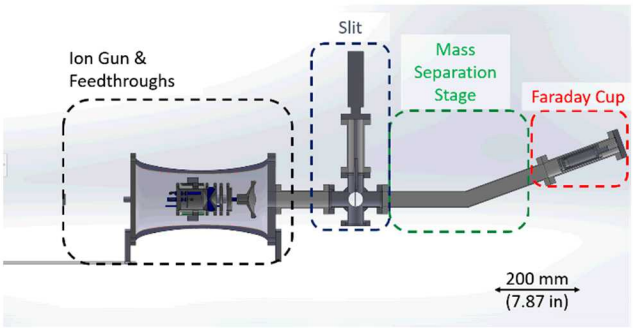

Figure 2: Cross-section of major IBSA systems, including ion gun, slit, bending arm of the mass separation stage, magnets (not shown) and Faraday cup.

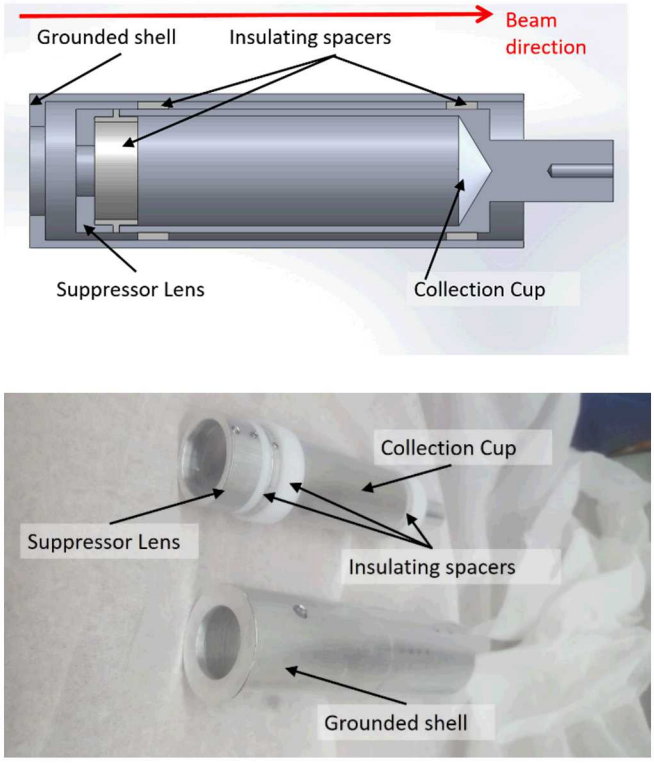

Figure 3: CAD drawing (top) and photograph (bottom) of Faraday cup used on the IBSA.

Figure 4: (Top) Slit mask mounted on a linear motion feedthrough and (bottom) D_2 beam as it passes through the mask.

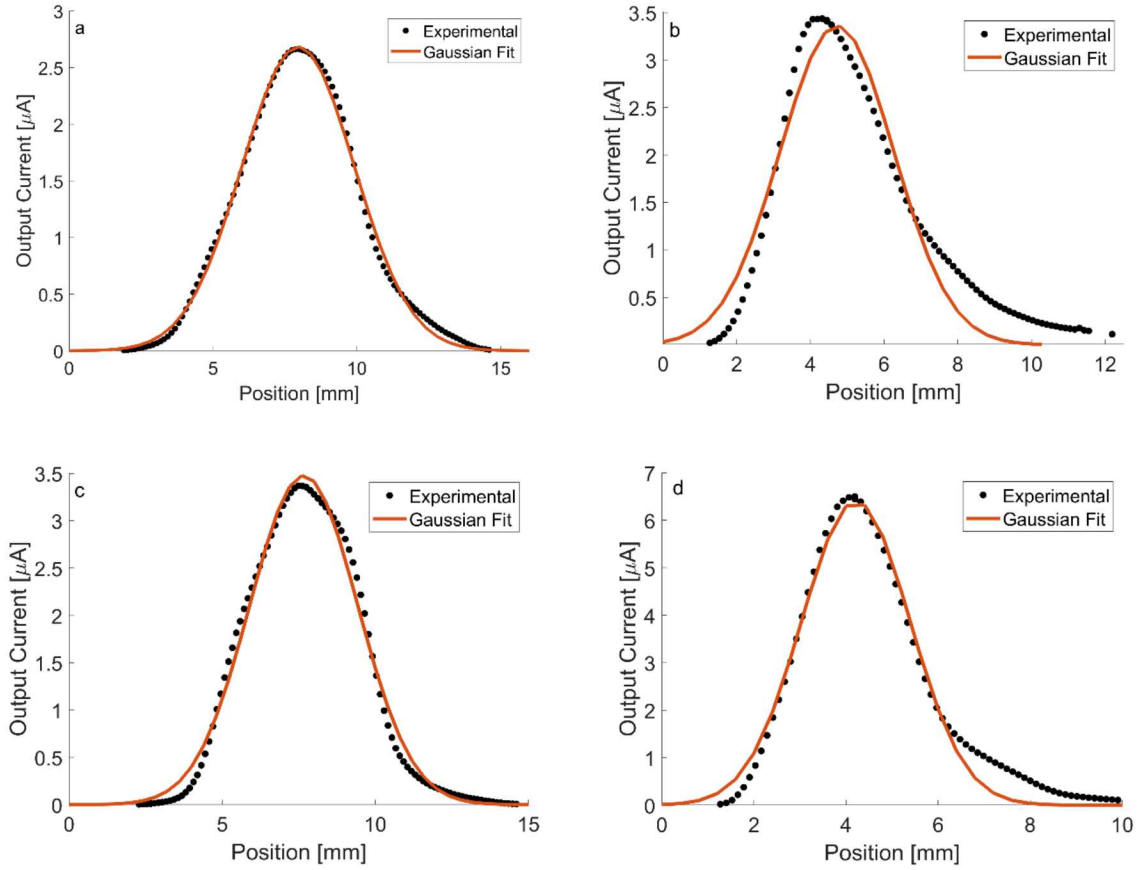

Figure 5: Measured spatial profiles and Gaussian fits of the He beam along the (a) x-axis and (b) y-axis. Measured and fit spatial profiles of the D beam along the (c) x-axis and (d) y-axis.

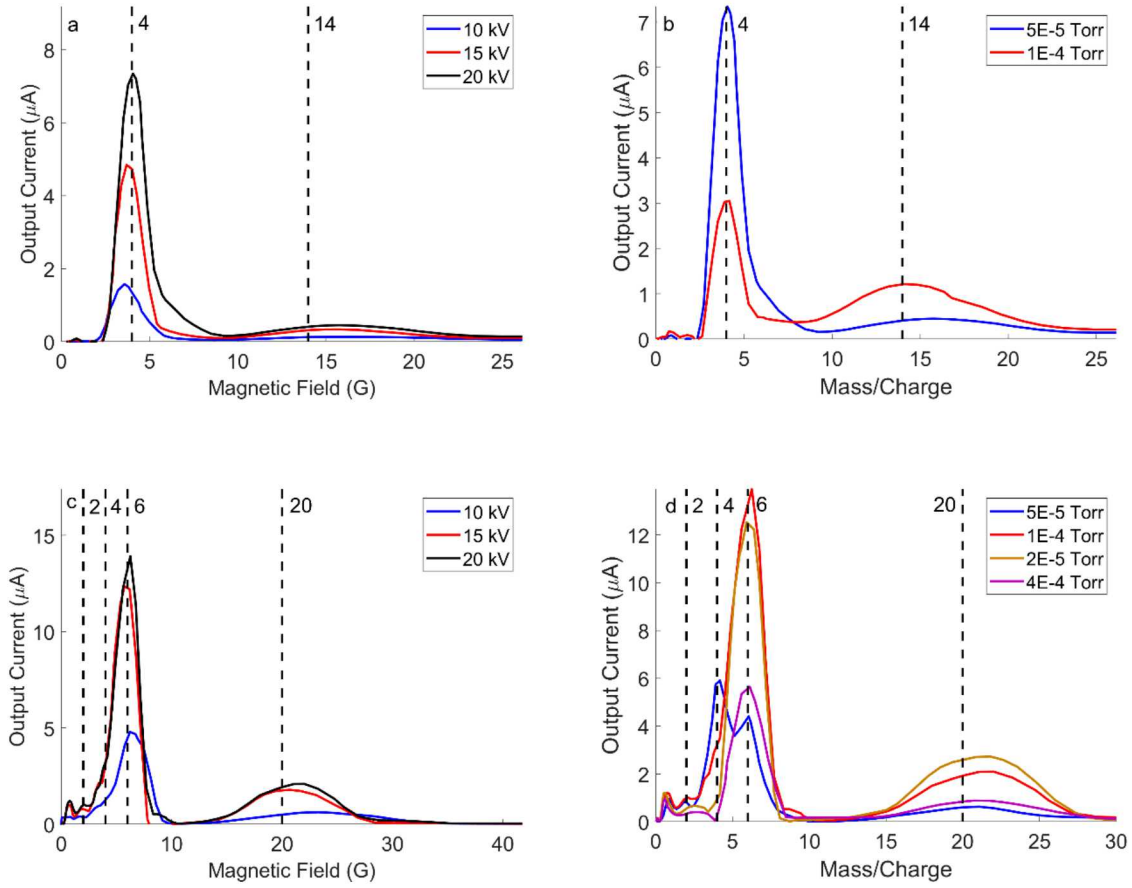

Figure 6: Magnetic analyzer profiles for the (a) He beam at 5×10^{-5} Torr, (b) He beam at 20 kV with significant mass peaks of 4 and 14 marked by vertical lines, (c) D_2 beam at 1×10^{-4} Torr, and (d) D_2 beam at 20 kV with significant mass peaks of 2, 4, 6, and 20 marked by vertical lines.

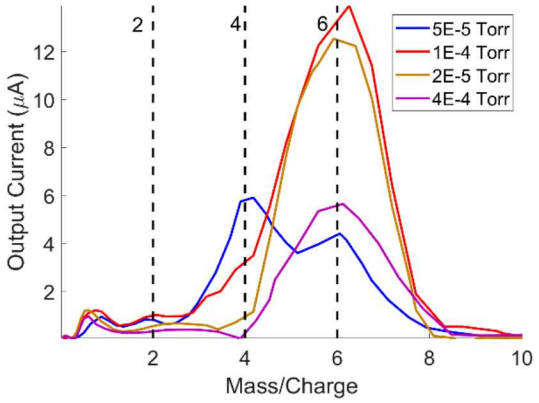

VI.

Figure 7: D_2 beam at 20 kV, zoomed into view the low mass peaks.

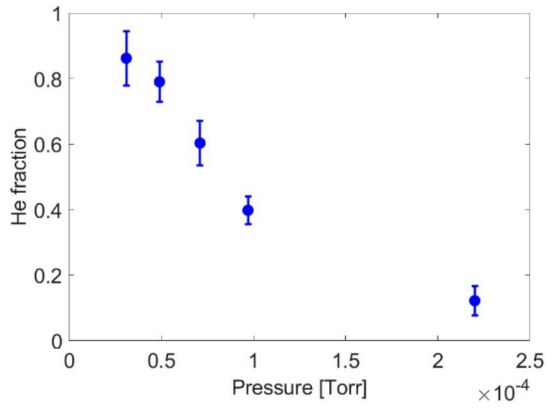

Figure 8: He^+ fraction as a function of P at 20 kV accelerating lens voltage.

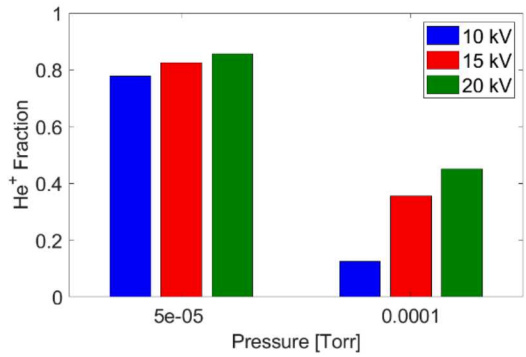

Figure 9: He^+ fraction vs pressures and accelerating lens voltage.

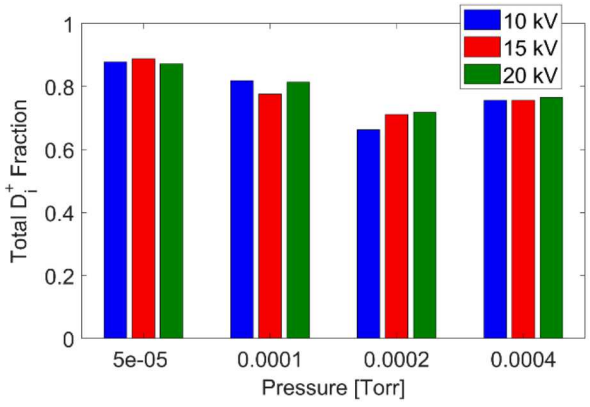

Figure 10: Total D_i^+ fraction vs pressure and accelerating lens voltage